PROCEEDINGS A

rspa.royalsocietypublishing.org

Research

Cite this article: Beatini V, Royer-Carfagni G, Tasora A. 2018 The role of frictional contact of constituent blocks on the stability of masonry domes. *Proc. R. Soc. A* **474**: 20170740. http://dx.doi.org/10.1098/rspa.2017.0740

Received: 24 October 2017
Accepted: 11 December 2017

Subject Areas:
structural engineering, civil engineering

Keywords:
masonry, domes, drum, tiburium, friction, non-smooth contact dynamics

Author for correspondence:
Gianni Royer-Carfagni
e-mail: gianni.royer@unipr.it

The role of frictional contact of constituent blocks on the stability of masonry domes

Valentina Beatini[1], Gianni Royer-Carfagni[2,3] and Alessandro Tasora[2]

[1]Department of Architecture, Abdullah Gül University, Sumer Kampus, Kocasinan 38280, Kayseri, Turkey
[2]Department of Engineering and Architecture, University of Parma, Parco Area delle Scienze 181/A, 43100 Parma, Italy
[3]Construction Technologies Institute, National Research Council of Italy (ITC-CNR), Via Lombardia 49, I 20098 San Giuliano Milanese (Mi), Italy

GR-C, 0000-0003-4879-9846

The observation of old construction works confirms that masonry domes can withstand tensile hoop stresses, at least up to a certain level. Here, such tensile resistance, rather than *a priori* assumed as a property of the bulk material, is attributed to the contact forces that are developed at the interfaces between interlocked blocks under normal pressure, specified by Coulomb's friction law. According to this rationale, the aspect ratio of the blocks, as well as the bond pattern, becomes of fundamental importance. To investigate the complex assembly of blocks, supposed rigid, we present a non-smooth contact dynamic analysis, implemented in a custom software based on the Project Chrono C++ framework and complemented with parametric-design interfaces for pre- and post-processing complex geometries. Through this advanced tool, we investigate the role of frictional forces resisting hoop stresses in the stability of domes, either circular or oval, under static and dynamic loading, focusing, in particular, on the structural role played by the underlying drum and the surmounting *tiburium*.

1. Introduction

The analysis of architectural masonry structures stems from the observation that they are usually massive. As the stress is much lower than the compressive strength,

THE ROYAL SOCIETY PUBLISHING

it is the geometric form and the organized association of the constituent elements that governs structural stability against the applied loads. A paradigmatic example is the segmental arch, made by appropriately shaped stone blocks. Coulomb proved that moment failure occurs when the *thrust line* can no longer be contained within the contouring surface of the arch. Kooharian observed that limit theorems for perfectly plastic solids could also be applied to structures formed by concrete voussoirs [1] under the hypotheses that the material is incapable of sustaining tension, can carry infinite compressive stress and that no sliding occurs at the interface, so that the only admissible motions are rotations about localized contact points or lines. Heyman [2] recognized that this result could be extended to masonry structures under the aforementioned assumptions.

Accordingly, the analysis of an arch is reduced to predicting the ultimate mechanism of a skeletal structure, usually two-dimensional, by using either graphical or analytical methods. A first extension of the thrust line analysis to domes and vaults was proposed in [3] by ideally interpreting the load-bearing mechanism as the composition of interacting arches in equilibrium, which identify localized networks of compressive forces. This is the *Thrust Network Analysis* of domes and vaults, which extends to the three-dimensional space the analogy between the catenary arch and the hanging cable by employing simulated cable nets to describe equilibrium, although from a computational point of view its implementation is very different from the calculation of a cable net. The method was further developed by Ochsendorf [4] and Block [5], using different operational approaches, either analytical or graphical [6]. Recently, Marmo & Rosati [7] have reformulated the original version by abandoning the role of the dual grid, elegantly employed in [5] to facilitate the use of this approach. The method reads for the three-dimensional flow of forces within the domes but, as its two-dimensional counterpart, it is conservative because it aims at finding at least one thrust net configuration where all the blocks are under compressive stress.

A simple membrane calculation indicates that domes with cylindrical symmetry made of no-tension material are biaxially compressed and thus remain sound from the crown down to a certain parallel (related to the thickness), beyond which they crack into 'slices' that act as flying buttresses [2]. This implies that the support structure (the drum) must resist to the inclined actions transmitted by the dome, i.e. besides the vertical, there is a horizontal component represented by the outward thrust. Such forces are often contained by one or more metal tension rings, as those installed by Luigi Vanvitelli in Saint Peter in Rome. In other cases, the drum is built so thick to contain the diagonal thrust, as in the Roman Pantheon. Such provisions confirm the validity of the zero-tensile strength assumption, but they all discard the geometrical and constitutive characteristics of the contact interfaces [8]. Indeed, many ancient domes over drum still stand up even without abutments, while the ancient tension rings, when present, often become slack over time, so that their action is negligible at least in the serviceability limit state.

It is our opinion that in order to fully understand the statics of real masonry domes, it is important to assume that a moderate tensile strength can counterbalance at least a part of the hoop stresses. Such strength is sometimes admitted as a property of the bulk material in a facilitation of the numerical analysis, rather than in an improvement of the accuracy of the response (see Sect. 2.2 of [9]). In fact, even if the single block may have a noteworthy tensile strength, the layered character of masonry and the fact that the mortar is not a sticky glue, suggest to neglect, presumably on the safe side, the possibility of developing any kind of tensile stresses. However, noteworthy shear forces of frictional nature can be generated at the interfaces. Therefore, the resistance to horizontal tensile forces in domes can be attributed to an effect of this kind, which depends on the vertical pressure in the way specified by Coulomb friction law.

A major difference between a theory that accounts for moderate tensile bulk strength and a theory based on frictional sliding of the blocks, consists in the fact that, for the latter, the aspect ratio and the bond pattern of the blocks forming the structure becomes of paramount importance for the determination of the collapse mechanism. In general, frictional laws can be associative or non-associative [10]. In the associative flow rule sliding is accompanied by a normal dilatancy, which can be interpreted by an assumed roughness of the contact profiles [11]. Experiments

have confirmed that also real dry frictional joints involve a moderate dilatancy [12], but in general the response is highly nonlinear, implying interactions among shear, torsion and bending moments [13].

In order to study the stability of complex arrangements, we assume that the blocks are rigid and in frictional contact, and we adopt a non-smooth contact dynamic (NSCD) approach [14] where the frictional flow rule is essentially non-associative *à la* Coulomb. Therefore, apart from the friction coefficient, the model is independent of constitutive data, which are always difficult to determine and subjected to a wide scattering. This results in a set-valued frictional contact model which is expressed through a differential variational inequality formulation [15,16], relying upon the theory of measure differential inclusion pioneered by Moreau [17,18]. In this setting, velocities are functions of bounded variation so that accelerations (and forces) are measures, a fact that accounts for the possibility of discontinuous events [19]. As in [20], we implement the model in a custom NSCD simulator based on the Project Chrono C++ software library, equipped with an optimized collision detection algorithm for convex and concave shapes. Moreover, in order to provide pre- and post-processing functionalities for the simulator, we developed custom tools within the Rhino CAD environment, using the Grasshopper parametric design software. Other authors [21–23] have successfully applied NSCD using, as an alternative, the LMGC90 software [24], which basically implements the same model, but here we prefer to rely upon our own code because, as developers, we have a deep access to the customization of the complementarity solver and of the collision detection engine. In detail, in order to solve complex problems with a great number of blocks in mutual contact, *ad hoc* improvements to the complementarity software and the collision detection engine had to be developed to speed up the convergence. Similarly, a smooth flow of data was developed between the simulator and the modelling tool. In any case, also the other results obtained with the LMGC90 software [25,26] confirm that the NSCD approach is an efficient and reliable way to study the failure mechanisms of masonry construction works. In fact, this approach can certainly analyse structures under dynamic loads, like a moving truck on an arch bridge but, remarkably, it can also determine the static state of block assemblies and provide information on the collapse mechanism under increasing applied loads [20]. In particular, the model can account for shear failures, a possibility that is ruled out in any approach based on the theorems of limit analysis, while the *effective* thrust network can be obtained from computation.

The plan of the article is the following. In §2, we briefly recall the NSCD approach and its formulation, detailing its numerical implementation. In §3, after discussing the role of frictional contact in providing an effective tensile strength to masonry, the implemented NSCD method is used to investigate the stability of various hemispherical domes, different in their aspect ratios and in the bond pattern of the constituent blocks, as well as in the possible presence of a *tiburium*, whose importance for the stability of the underlying drum will be discussed in detail. Section 4 discusses how the frictional contacts interfere with the geometric proportions, both at the local level (aspect ratio of the constituent blocks) and at the global level (the shape of the dome, either circular or oval). The overall achievements, drawbacks and hints for future work are discussed in §5.

2. The non-smooth contact dynamics formulation

Apart from *ad hoc* improvements to the solver to speed up the convergence, the NSCD model considered here is the same used in [20]. Referring to this for the details, here we just recall the basic aspects, necessary for the physical interpretation of the numerical results presented in the sequel. We recall that the NSCD formulation is characterized by non-smooth mechanics laws, defined through convex but not necessarily differentiable potentials, for which sub-differentials and measure differential inclusions [17,18] are basic tools [27]. To account for non-smooth trajectories and jumps in speeds induced by hard contacts, the positions $\boldsymbol{q}(t)$ are functions *absolutely continuous* with respect to the Lebesgue measure in time, but velocities $\boldsymbol{v}(t)$ are *functions of bounded variation*.

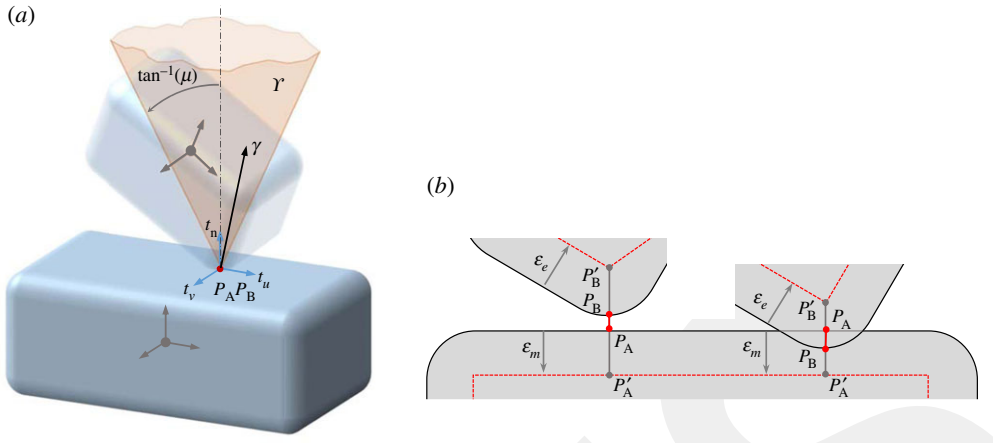

Figure 1. The contact model. (*a*) The Coulomb friction cone for a single contact (local reference system associated with the upper block). (*b*) Robust handling of contacts using sphere-swept surfaces. (Online version in colour.)

At the *i*th contact point of the generic block, define a local coordinate system by one normal unit vector $\boldsymbol{t}_{\mathrm{n},i}$, directed inwards, and two mutually orthogonal tangent vectors $\boldsymbol{t}_{u,i}, \boldsymbol{t}_{v,i}$. The contact force exerted on the block is defined by the force multipliers $\hat{\gamma}_{\mathrm{n},i}$ for the normal component, and $\hat{\gamma}_{u,i}, \hat{\gamma}_{v,i}$ for the tangential forces caused by friction, so that the contact force reads

$$\boldsymbol{F}_i = \boldsymbol{F}_{\mathrm{n},i} + \boldsymbol{F}_{\parallel,i} = \hat{\gamma}_{\mathrm{n},i}\boldsymbol{t}_{\mathrm{n},i} + \hat{\gamma}_{u,i}\boldsymbol{t}_{u,i} + \hat{\gamma}_{v,i}\boldsymbol{t}_{v,i}, \tag{2.1}$$

where $\boldsymbol{F}_{\mathrm{n},i}$ and $\mathrm{t}\boldsymbol{F}_{\parallel,i}$ are the normal and tangential components, respectively.

The Coulomb–Amontons contact model introduces the friction coefficient μ and states that the contact reaction is contained in the convex cone shown in figure 1*a*, defined by $\mu\hat{\gamma}_{\mathrm{n},i} \geq \sqrt{\hat{\gamma}_{u,i}^2 + \hat{\gamma}_{v,i}^2}$ for $\hat{\gamma}_{\mathrm{n},i} \in \mathbb{R}^+$. Moreover, the tangential relative velocity $\mathbf{v}_\parallel$ and the tangential contact force $\boldsymbol{F}_\parallel$ are in opposite direction, i.e. $\langle \boldsymbol{F}_\parallel, \mathbf{v}_\parallel \rangle = -\|\boldsymbol{F}_\parallel\| \|\mathbf{v}_\parallel\|$. No distinction is made here between static μ_s and kinetic μ_k friction coefficients because, even if the formulation could support this, it would have no significant outcome for incipient potential motions of masonry structures, being the sliding either null (in static analyses) or moderate (in transient seismic analyses).

For active contacts, the De Saxcé bipotential [27] allows defining in a synthetic and elegant form the conditions governing the frictional force as a cone complementarity problem, which result in a convenient numerical implementation. Let $\boldsymbol{f}(\boldsymbol{q}, \boldsymbol{v}, t)$ denote the generalized forces, including gravitational forces, external applied forces, gyroscopic forces, let M represent the mass matrix, containing all the masses and inertia tensors of the rigid bodies, and let $\boldsymbol{f}_\mathrm{c}$ represent set-valued contact forces, given by multipliers $\hat{\gamma}_{\mathrm{n},i}$, $\hat{\gamma}_{u,i}$ and $\hat{\gamma}_{v,i}$. The equilibrium condition for all blocks is stated by

$$M\frac{\mathrm{d}\boldsymbol{v}}{\mathrm{d}t} = \boldsymbol{f}(\boldsymbol{q}, \boldsymbol{v}, t) + \boldsymbol{f}_\mathrm{c}. \tag{2.2}$$

In an approach based on measure differential inclusions, one can allow for discontinuous velocities $(\boldsymbol{v}^{(l+1)} - \boldsymbol{v}^{(l)})$ over a time step h, which are determined by the reaction impulses $\boldsymbol{\gamma}_i = \int_t^{t+h} \mathrm{d}\boldsymbol{\gamma}_i(\mathrm{d}t)$ (see expressions (28–30) of [20]).

Because the integration process may be affected by various numerical inaccuracies (integration error, finite precision of floating point, etc.), a peculiarity of the code is the introduction of a stabilizing term, referred to as $\boldsymbol{b}$ in [20], which corrects the relative position of blocks at the active contacts at each time step, so that possible compenetrations are always maintained within a prescribed tolerance.

In extreme synthesis, time integration is performed with a stepping scheme; at each time step, one must compute the unknown vector $\boldsymbol{\gamma}$ which collects contact impulses $h\hat{\gamma}_{\mathrm{n},i}$, $h\hat{\gamma}_{u,i}$ and $h\hat{\gamma}_{v,i}$

from (2.1). This represents the main bottleneck, as $\boldsymbol{\gamma}$ must be obtained by solving a difficult cone complementarity problem $\boldsymbol{\gamma} \in \Upsilon \perp \underline{\bar{\boldsymbol{u}}} \in \Upsilon^*$, where Υ is the set of all friction cones, Υ^* is its dual, and $\underline{\bar{\boldsymbol{u}}}$ is a nonlinear term that, following the notation of [20] (see formula (35)), is given by

$$\underline{\bar{\boldsymbol{u}}} = N\boldsymbol{\gamma} + \boldsymbol{r} + \tilde{\boldsymbol{u}}(\boldsymbol{v}), \tag{2.3}$$

where N depends upon the mass matrix M and the configuration of contacts; $\boldsymbol{r}$ depends upon the mass matrix, the stabilizing term $\boldsymbol{b}$, the applied forces and the multipliers $\boldsymbol{\gamma}$; and finally $\tilde{\boldsymbol{u}}(\boldsymbol{v})$ is a highly nonlinear function of the velocity field $\boldsymbol{v}$.

To bypass the noteworthy numerical difficulties of solving such nonlinear complementarity problem, one may neglect the $\tilde{\boldsymbol{u}}$ term of (2.3). This leads to a more treatable cone complementarity of convex nature (expression (36) of [20]), at the cost of accepting that the frictional model becomes *associative*. From a physical point of view, omitting $\tilde{\boldsymbol{u}}$ in (2.3) implies that a small gap proportional to $h\|\mathbf{v}_{i,\|}\|\mu$, where $\mathbf{v}_{i,\|}$ is tangential relative velocity at the active contact point, builds up during sliding motion [28]. However, the introduction of the stabilizing term $\boldsymbol{b}$ annihilates this gap at the end of the iteration. In other words, the solution of the problem relies on an associative frictional model at the time-step level, but the dilatation effect remains limited to the magnitude associated with one time step, so that in the long run the solution is equivalent to that of a *non-associative frictional model*. The magnitude of the dilatation tends to zero for $h \downarrow 0$ and becomes negligible as the tangential sliding velocity $\mathbf{v}_{i,\|}$ tends to zero, as it is the case when the blocks are in equilibrium under static loads, i.e. their movement is small and serves to provide the settlement of the system in order to develop the frictional contact forces. This convex relaxation from the associated friction law has clearly no importance in the cases in which $\boldsymbol{v} = \mathbf{0}$ and consequently $\tilde{\boldsymbol{u}}$ vanishes, i.e. for static problems or sticking or rolling contacts without slip.

Efficient numerical solution algorithms can be used to solve the convex cone complementarity problem. Here, we employ a variant of the non-monotone spectral projected gradient method [29] equipped with preconditioning and a fall-back strategy to ensure monotone convergence [30]. In order to decide if the set of blocks is in equilibrium under static loads with no appreciable movements, one solves the cone complementary problem at step $(l + 1)$ assuming that the relative velocity field at step (l) is null, calculates the contact forces and verifies *a posteriori* if this solution is compatible with null velocity at step $(l + 1)$. If this is not the case, then the blocks shall move.

Another peculiarity of the code is the computation of the contact points, which can be quite difficult in case of complex geometries, as considered in the following. The collision pipeline is split in a *broad phase*, which sorts out, at low computational costs, only those pairs of blocks that are close enough to potentially generate contact points, followed by a successive *narrow phase*, which refines those pairs. For the broad phase filtering, we adopt the bounding volume hierarchy implemented in [31] that, for structures of the kind analysed in the sequel, provides a collision algorithm of quasilinear time complexity. The narrow phase stage is based on the Gilbert–Johnson–Keerthi algorithm [32] that operates on convex surface (boxes, faceted polytopes, cylinders, etc.). The geometries that we will consider are strongly characterized by degenerate cases, i.e. where two faces are coplanar and there are infinite contact points. This difficulty is solved by running the Gilbert–Johnson–Keerthi algorithm several times with small perturbations on object rotations and keeping a persistent contact manifold, thus obtaining a set of possible contact points from which those that maximize the contact patch are selected by a heuristic collision filtering step.

A second problem is that the Gilbert–Johnson–Keerthi algorithm assumes shapes to be separated, but time-step integration and numerical errors might involve slight interpenetration. To overcome this problem, we consider the original shapes as sphere-swept surfaces, like the one represented in figure 1*b*, obtained with the algorithm proposed in [33]. Offsetting the original contours of the blocks of a quantity ε, one defines a tolerance distance for the contacts, i.e. two blocks are assumed to be in contact if the interpenetration is less than ε, as schematically indicated in figure 1*b*. This ensures the robustness of the contact detection algorithm.

The model provides multiplicity of solutions for dual variables (the contacts), but gives a unique solution in terms of primal variables (the velocities) [34]. This indeterminacy does not affect the trajectories of falling blocks, but may be a problem for the iterative solver because iterations may converge to different solutions especially when the blocks are in equilibrium, showing a fluctuation of the contact forces. For these reasons, we regularize by adding a numerical compliance for the contacts, here achieved by modifying the matrix N of (2.3) by adding a diagonal part. Roughly speaking, regularization is somehow equivalent to introducing a fictitious extensional spring between impinging bodies at each contact point. Our numerical tests [35] showed that the higher the compliance parameter, the faster the convergence of the iterative solver, but even a very low value of the compliance provides good stability even for large time steps.

On the one hand, the fictitious compliance could be calibrated to model the presence of mortar joints between the blocks. However, a precise calibration can be difficult to achieve because there are various types of mortars with different mechanical properties, essentially nonlinear. Moreover, in the following numerical experiments, we do not model the single bricks of the masonry works (otherwise the presence of hundreds of thousands of elements would expand the computation time too much), but rather we consider macro-blocks that simulate sets of smaller bricks, for which the evaluation of the role of the mortar can be difficult. Therefore, we have decided to consider a very low, non-physical value of the compliance, compatible with an engineering assumption of pseudo-rigid contacts. We have verified that results do not sensibly change if the selected value of the compliance is increased, or reduced, of one order of magnitude.

In any case, we observe that NSCD simulations might exhibit sensitivity to input data, especially for large motions caused by seismic actions like those of §3c. For instance, when simulating collapses, small changes in the geometry might give different outcomes in terms of collapse configuration, especially when starting from complex shapes. This is not a drawback of the numerical procedure, but a property inherent to the nature of the physical problem. In static analysis, however, this sensitivity issue is less relevant, and is mostly associated with the problem that the assumption of rigid blocks causes an indeterminacy of over-constrained contact forces; hence small changes in the input data might cause slightly different networks of contact forces, but still produce the same static outcome. We resolve this issue through the aforementioned regularization, which avoids indeterminacy in the redundant contact constraints and, at the same time, reduces the sensitivity of results to input data.

3. Experiments on hemispherical domes

Referring to the illustrative example of a hemispherical dome supported by a slender cylindrical drum, the aim of this section is to show the significant role played by the frictional nature of the contact interactions among the constituent blocks of the masonry work in providing an effective tensile strength.

(a) A simple analytical approach

It is useful to refer to the simple analytical treatment of a hemispherical dome. Let R and s represent the radius of the mid surface and the (constant) thickness of the dome, respectively. Reference can be made to the membrane theory, first proposed by Schwedler in 1866 and later developed by other authors including Rankine (1904) [2]. Besides geometric and loading symmetry, the basic hypotheses are that the surface is so thin that its bending stiffness is negligible and the internal forces are coplanar. Figure 2*a* shows the geometric parameters θ and φ for a spherical cap, with $0 \leq \theta \leq 2\pi$ and $0 \leq \varphi \leq \alpha$, which becomes hemispherical for $\alpha = \pi/2$. If ρ denotes the density of the material and g the gravity acceleration, it is a standard argument to

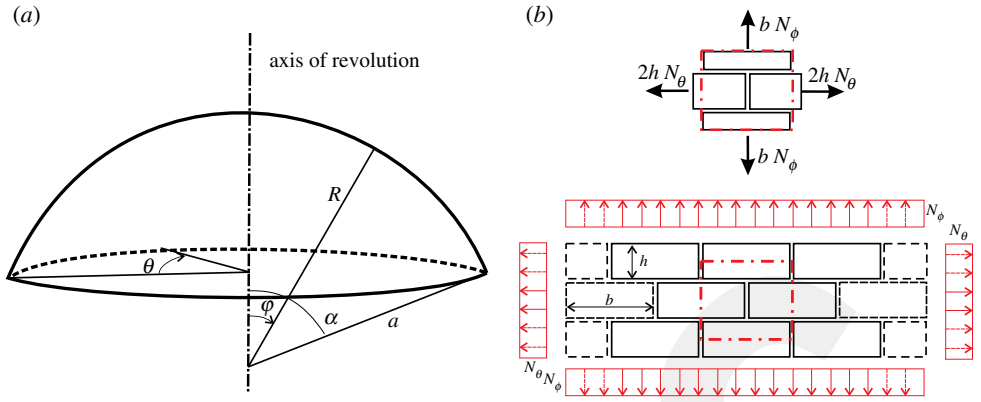

Figure 2. Analytical treatment of a hemispherical dome. (*a*) Parameter definitions. (*b*) Schematic of the bond pattern: frictional contact allows carrying hoop stresses. (Online version in colour.)

demonstrate that the meridian and hoop stress resultants, N_ϕ and N_θ, respectively, in units of force *per* length, read

$$N_\phi = -\rho s g \frac{R}{1+\cos\varphi} \quad \text{and} \quad N_\theta = \rho s g R \left(\frac{1}{1+\cos\varphi} - \cos\varphi \right). \tag{3.1}$$

These expressions provide the well-known result that, whereas the meridian stress is always compressive, the hoop stress becomes tensile when $\varphi > \bar{\varphi} \simeq 0.90\,\text{rad} \simeq 51.8^\circ$.

Let us suppose that the dome is formed by layering successive rings in an interlocking bond pattern, such that the ends of each block are approximately above the centre of the blocks beneath it. With respect to the schematic of figure 2*b*, let the width and height of each block be b and h, respectively, with $b, h \ll R$. Consider the equilibrium of a representative volume element of sides b and $2h$, as represented in the same figure. Taking into account that the hoop stress can only be equilibrated through the frictional contact of the interfaces, if μ denotes the friction coefficient, then from (3.1) the joint will not slide if

$$2hN_\theta \le \mu(-bN_\phi) \;\Rightarrow\; \mu \frac{b}{2h} \ge \sin^2\varphi - \cos\varphi. \tag{3.2}$$

On the other hand, if σ_r denotes the tensile strength of the material forming the block, the condition to avoid rupture is

$$2hN_\theta \le sh\sigma_r \;\Rightarrow\; 2\rho g R \frac{\sin^2\varphi - \cos\varphi}{1+\cos\varphi} \le \sigma_r. \tag{3.3}$$

In a hemispherical dome, the maximum tensile hoop stress is at the base, for $\varphi \simeq \pi/2$. Consequently, from (3.2) and (3.3), one finds that neither sliding nor rupture will occur provided that conditions

$$\frac{2h}{b} \le \mu \quad \text{and} \quad R \le \frac{\sigma_r}{2\rho g} \tag{3.4}$$

are satisfied. The first condition poses a limitation on the aspect ratio of the blocks, whereas the second one affects the size of the dome.

Setting as representative values $\sigma_r = 2\,\text{MPa}$, $\rho = 1.8 \times 10^3\,\text{kg m}^{-3}$ and $g = 9.81\,\text{m s}^{-2}$, one obtains from $(3.4)_2$ the condition $R \le 56.6\,\text{m}$, which is verified in all cases of practical interest. On the other hand, condition $(3.4)_1$ is more difficult to be satisfied because, in general, the friction coefficient is of the order of $\mu = 0.4 \div 0.6$. This simplified approach shows that, at least at the qualitative level, the wider the blocks, the higher is the hoop stress that can be sustained *via* frictional contact. To this respect, it may be interesting to observe that the major masonry

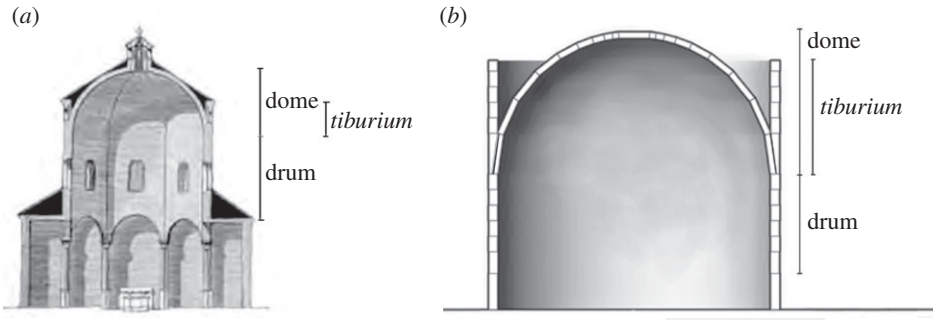

Figure 3. (*a*) The Baptistry of the Cathedral of Novara, Italy, an exemplary dome with drum and *tiburium*. (*b*) Cross section of the model with evidence of the blocks fitting the base of the hemispherical dome, the drum and the *tiburium*.

constructions in Rome, from the imperial time to the baroque period, were made of bricks called *pianelle* (flat tiles), about 16 cm long and 4 cm thick, so that $2h/b = 0.5$.

It is certainly very important to recognize what the boundary conditions are at the springing of the dome. If the support cannot move outwards, it confines and constrains the movement of the first ring of blocks. On the contrary, if the contact between the dome and the support is frictionless or, equivalently, the support cannot constrain outward movements, the frictional contribution at the lower interface is missing and the no-sliding condition $(3.4)_1$ becomes $4h/b \leq \mu$. In order to improve the performance of the dome, it is thus crucial to provide a sufficiently rigid support and, possibly, to increase the meridian stress at the springing, to enhance the frictional strength at the interfaces.

The above arguments indicate that a hemispherical dome is prone to loosen and open at the base due to a partially unbalanced tensile hoop stress. However, the dome does not completely crack into 'slices', forming flying buttresses, because a part of the hoop stress can be carried through frictional contact, usually at the price of frictional sliding. Though the resulting state of stress is quite complicated, it can be seen that, in the case of frictional sliding, a moderate outward radial thrust may be transmitted to the underlying supporting structure.

(b) Numerical experiments: dome, drum and *tiburium*

In the assemblies of rigid blocks considered hereinafter, there are three main architectural elements: the dome itself, the drum (or *tympanum*) supporting the dome and the *tiburium*, i.e. a cylinder that ideally extends the drum upward, enclosing the dome. These are illustrated in figure 3*a* through a section view of the Baptistry of the Cathedral of Novara, Italy, dating back to the beginning of the fifth century. It is important to recall that the *tiburium* is usually considered a mere architectural element, with its surrounding walls supporting a roof that hides the dome from the outside,[1] but its important *static* role has also been recognized with reference to a thrust network analysis that considers the dome as composed of independent lunes [3]: the *tiburium* adds weight, so that the thrust line of each lune, acting as a pie-shaped semi-arch, remains within the section of the dome in the proximity of the base, where it curves downward. However, we will show that another important effect of the *tiburium* is that of compressing the drum in such a way that, for an interlocked bond pattern as in figure 2*b*, hoop stresses can be equilibrated thanks to frictional contact.

The considered geometry is that of a hemispherical dome, of internal radius 7 m and thickness 0.3 m, composed of 10 rings and one keystone crown block, constructed in such a way that, in the plan view, the parallels delimiting the rings are concentric circles. The dome is supported

[1]The *tiburium* should not to be confused with the lantern, which is a little cylindrical element atop the dome, providing natural light inside.

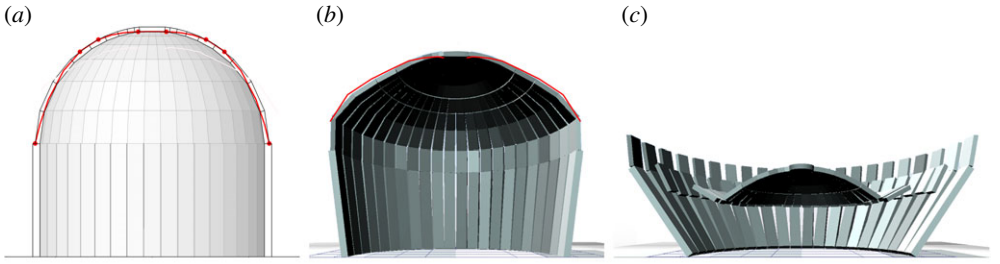

Figure 4. Dome made by a series of independent lunes, with a drum formed by independent slender columns and no *tiburium*. (*a*) Section layout and conventional thrust line. (*b*) Collapse mechanism from the NSCD simulation and effective thrust line after 1 s. (*c*) Deformation at $t = 2$ s. (Online version in colour.)

by a drum of thickness 0.45 m and height about 5 m. The friction coefficient is set equal to $\mu = 0.4$ in all simulations. The structure is supposed to be loaded by its own weight, with density $\rho = 1800\,\mathrm{kg\,m^{-3}}$. The dome may be enclosed, or not, by a *tiburium*, supposed of the same internal diameter and thickness of the drum. The shape of the blocks fitting the junction among dome, drum and *tiburium* is represented in the cross section of figure 3*b*.

In the NSCD simulations, the dead weight is instantaneously applied at the reference time $t = 0$. This may seem quite unrealistic: all architects of the past were very careful in removing the scaffoldings gradually in order to avoid undesired movements, waiting for a complete settlement of each individual layer under its own weight. Moreover, when domes were built without falsework by layering one ring above the other, the construction phase induced a particular redistribution of stresses that is neglected here. If the blocks were perfectly rigid and in dry contact, the time in which the dead load is applied would be of little importance provided that the structure can withstand it without appreciable movements. However, as discussed in §2, the regularization procedure is equivalent to the introduction of a compliance between the blocks that somehow simulates the deformation of the mortar joints. On the one hand, a sensitivity analysis for the consequent deformation of the dome, which may certainly influence its collapse, has not been done. On the other hand, the very small value of the effective compliance that has been used here leads us to conjecture that the effect is not substantial, as tentatively confirmed by the comparisons of numerical simulations with different values of the compliance. In any case, as in the following we will take the collapse time as a basic variable to measure the effectiveness of the structure, the fact that the load is instantaneously applied gives to our analysis the character of a first approximation.

The first considered case is a dome without *tiburium* made by a series of independent pie-shaped semi-arches (lunes), supported by a drum clearly unable to withstand any hoop stress because formed by independent, slender columns. In figure 4*a*, we draw over the cross section the *conventional* thrust line, obtained with the classical method *à la* Méry. With a thickness over span ratio less than 1/45, the conventional thrust line lays slightly outside the arch profile but, more importantly, outward horizontal thrusts are transmitted by the arches to the drum. The NSCD simulation shows that the structure collapses due to its inability to balance this action. Figure 4*b* reports the deformed section from the NSCD simulation at $t = 1$ s, over which we have plotted the *effective* thrust line at that instant, defined as the envelope of the resultants of the calculated forces at each contact plane between adjacent blocks, as calculated by the numerical code. The failure sequence is completed by figure 4*c* referring to $t = 2$ s.

To equilibrate the outward thrust, it is customary to insert a metal tension ring at the base of the dome. For the same bond pattern of figure 4, a condition of this type has been simulated by connecting any pair of adjacent blocks of the lowest masonry course with springs constraining the opening of the meridian interfaces. Assuming a spring coefficient $k = 103\,\mathrm{kN\,mm^{-1}}$, equivalent to a steel chain of diameter $\phi = 25$ mm, the NSCD analysis predicts that the structure is safe because

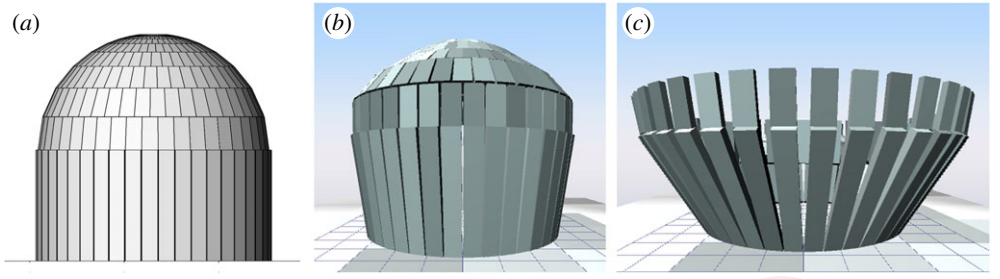

Figure 5. Dome with interlocked bond pattern, supported by a drum formed by independent slender columns and no *tiburium*. (*a*) Layout. Predicted mechanism at (*b*) $t = 1$ s and (*c*) $t = 2$ s. (Online version in colour.)

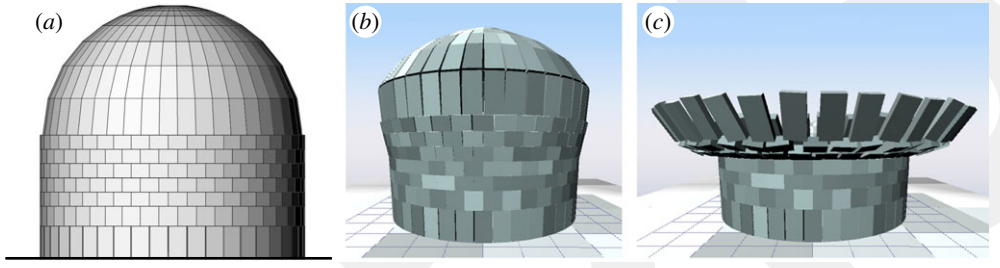

Figure 6. Dome with no *tiburium* made by a series of independent lunes, supported by an interlocked drum. (*a*) Layout. Predicted collapse mechanism at (*b*) $t = 1$ s and (*c*) $t = 2$ *s*. (Online version in colour.)

the hoop stress from the chain can re-centre the thrust line. Without such a ring, one may wonder if the dome can equilibrate the hoop stress thanks to frictional contact by interlocking the blocks as in figure 5*a*. The deformations represented in figure 5*b*,*c* for $t = 1$ and $t = 2$ s, i.e. at the same time steps of figure 4, indicate that there is no sensible improvement with respect to the previous case. The reason is that for the blocks at the base of the dome, the aspect ratio is $2h/b = 4$, so that condition (3.2) is certainly not satisfied. The drum, formed by independent slender columns, provides no confinement.

The complementary case, when the drum is interlocked (aspect ratio $2h/b = 1$) while the dome is made of independent arches, is depicted in figure 6*a*. The outward collapse mechanism of the drum, represented in figure 6*b*,*c* at the same time steps $t = 1$ and $t = 2$ s, indicates that the weight of the dome is not able to impart to the drum, through frictional contact, a sufficient resistance to hoop tensions. Nevertheless, the drum does not completely tip over.

The same conclusions are valid for the layout of figure 7*a*, where both dome and drum are interlocked, even if the collapse snapshots at $t = 1$ and $t = 2$ s, represented in figure 7*b*,*c*, show that the movement is slightly slower. It should be mentioned that, according to our interpretation of the resistance against cracking and collapse from the friction between the dome's layers, it makes a difference whether the layers lay on conical surfaces perpendicular to the dome's meridian lines, as in all the cases considered here, or on horizontal planes, as for example in the trulli [36]. In fact, in the first case, the tangential component of the applied force is lower than in the second case, even if the difference tends to vanish for those rings close to the drum, i.e. where the resistance to the hoop stress is determinant.

It may be useful to add a *tiburium* over the drum. What needs to be recognized now is whether its main effect is that of centring the thrust line where it curves downward at the springing of the dome, or that of increasing the capacity of the drum to withstand hoop stresses thanks to frictional contact. Therefore, consider first the layout of figure 8*a* (some blocks are hidden for visual clarity), identical to that of figure 4*a* except for the *tiburium*. Again, no hoop stress can be sustained by a

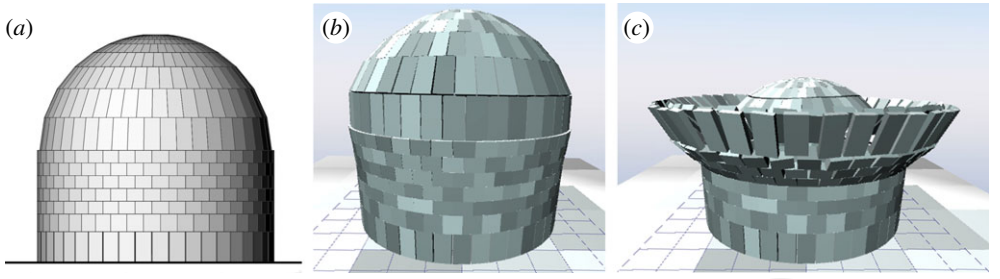

Figure 7. Dome and drum with interlocked bond pattern and no *tiburium*. (*a*) Layout. Predicted collapse mechanism at (*b*) $t = 1$ s and (*c*) $t = 2$ s. (Online version in colour.)

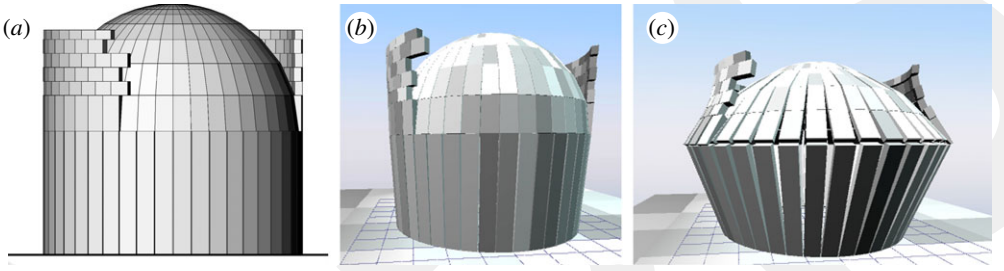

Figure 8. Dome with independent lunes on a drum formed by independent slender columns and interlocked *tiburium*. (*a*) Layout. Calculated collapse mechanisms at (*b*) $t = 1$ s and (*c*) $t = 2$ s. (Online version in colour.)

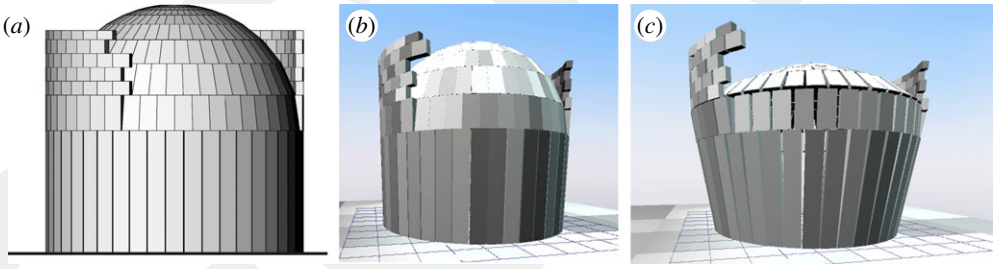

Figure 9. Interlocked dome and *tiburium* on a drum with independent slender columns. (*a*) Layout. (*b*) Deformation at $t = 1$ s. (*c*) Collapse mechanism at $t = 6$ s. (Online version in colour.)

drum formed by slender independent columns, so that the only function of the *tiburium* shall be that of modifying the line of thrust in the independent lunes forming the dome. From the NSCD simulations, represented in figure 8*b*,*c* at $t = 1$ s and $t = 2$ s, respectively, the main conclusion is that the added weight is not sufficient to drive the thrust line within the profile of the dome and, consequently, the structure collapses with no apparent benefit with respect to the case of figure 4*c*.

Figures 9 and 10 are the counterparts of figures 5 and 6 with the *tiburium*. The snapshots of the NSCD simulations taken at $t = 1$ s, represented in figures 9*b* and 10*b*, indicate very small displacements, but the former is not stable, while in the latter large cracks occur without collapse. This is clear from figures 9*c* and 10*c*, showing the results at $t = 6$ s. Evidently, the dome becomes much more stable when it is the drum, rather than the dome itself, to be formed with an interlocked bond pattern. In fact, the increase of meridian stress produced on the dome by the weight of the *tiburium* is relatively small as the greatest part of such weight flows directly to the underlying drum (cf. figure 3*b*). The conclusion does not substantially differ when the blocks of

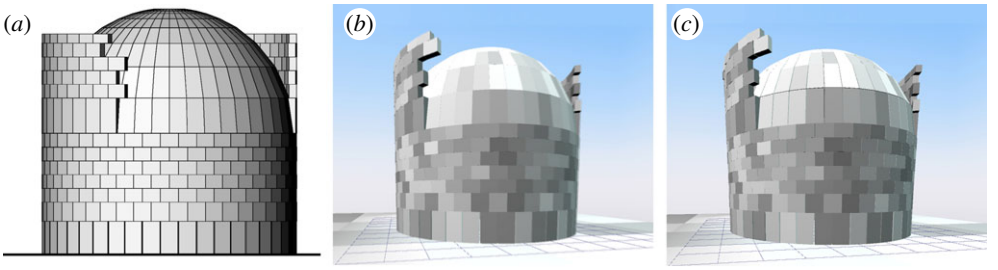

Figure 10. Dome made by independent lunes, with interlocked drum and *tiburium*. (*a*) Layout. (*b*) Deformation at $t = 1$ s. (*c*) Opening of cracks at $t = 6$ s without collapse. (Online version in colour.)

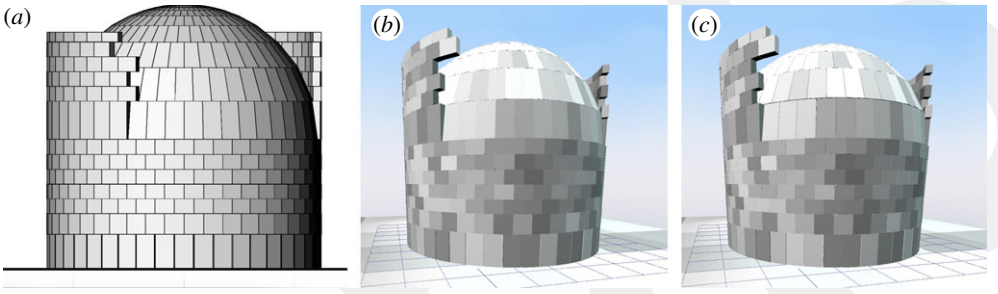

Figure 11. Dome drum and *tiburium* with interlocked bond pattern. (*a*) Layout. Deformation at (*b*) $t = 2$ s and (*c*) at $t = 6$ s. (Online version in colour.)

the dome, the drum and *tiburium*, are all interlocked, as in figure 11*a*. The NSCD simulations again at $t = 2$ s (figure 11*b*) and at 6 s (figure 11*c*) are comparable with those of figure 10. Indeed, the dome is made by narrow blocks ($2h/b \simeq 4$) so that the contribution of friction is limited.

These examples indicate that the role of the *tiburium* is not limited to redirecting the thrust line, but also comprehends the activation of frictional forces by increasing the normal stress in the drum, being the second contribution the more important the lighter the dome is. Observing the elegant *tiburium* structures built over very slender domes by architects like Borromini, one may wonder if the ancient masters had already recognized, albeit intuitively, this important effect.

(c) Dynamic response

The NSCD approach can model the dynamic effects due to the movement of the ground as during an earthquake. The considered layout is identical with that of figure 11 (interlocked dome, drum and *tiburium*), apart from a slight increase in height (8.5 m) of the *tiburium*. A global orthogonal reference system is introduced such that $x - z$ is the ground plane, and y the vertical axis. In the simplest case, a sinusoidal motion is applied to the ground with amplitude $A = 0.033$ m and frequency $f = 1.5$ Hz, so that the peak ground acceleration (PGA) is $0.3g$. For a motion applied in the direction x, figure 12*a* shows sequential pictures of the moving structure after 1, 3 and 5 s. As the oscillations of the ground shake the structure, diminishing as well the frictional interface forces due to internal collisions, the drum, able to balance the thrust from the dome in the static case, looses part of this capability and opens up, carrying down the surmounting *tiburium* in this motion. The dome, not any more confined at the base, collapses.

Figure 12*b* records the plots, as a function of time, of the displacement of the ground in x-direction ($d_{g,x}$), as well as the displacement of the centroid of a block of the dome located right over the springing, marked with a dot in figure 12*a* ($d_{b,x}$ and $d_{b,z}$ components). Clearly, $d_{b,x} - d_{g,x}$ is the displacement of the same block for an observer fixed on the ground. Looking at the

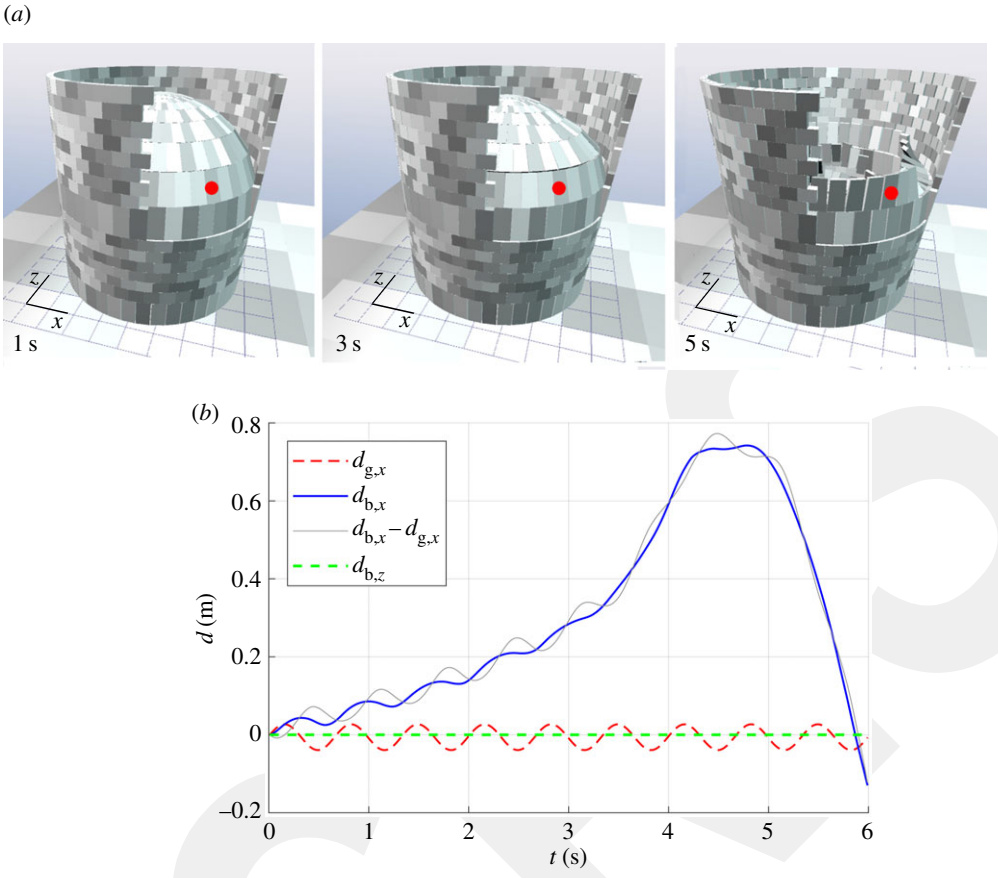

Figure 12. Interlocked dome, drum and *tiburium*, under *x*-direction oscillatory ground displacement (PGA 0.3 g, $f = 1.5$ Hz). (*a*) Failure steps $t = 1$ s, $t = 3$ s and $t = 5$ s. (*b*) Displacement of the ground ($d_{g,x}$) and of the block marked with a dot in *x* ($d_{b,x}$) and *z* ($d_{b,z}$) directions. (Online version in colour.)

location of such a block, it is not surprising that the $d_{b,z}$ component is almost null, because in the *z* direction, at right angle to the direction of the ground acceleration, the block is constrained by the contact of the neighbouring elements. Along the *x*-direction, the graph of $d_{b,x}$ shows oscillations that follow the ground motion, but since the dome expands during collapse, the displacement reaches the value corresponding to the case in which the block lies on the ground.

Because the *tiburium* usually supports a gabled roof spanning over the dome, it is worth investigating if the capacity of the *tiburium* under horizontal actions can be increased by confining it at the top by a horizontal diaphragm. The model is represented in figure 13*a*, where a monolithic 0.8 m thick block closes the *tiburium*. Comparing the snapshots from the NSCD simulations with their counterparts of figure 12*a*, at the same time, one may deduce that, at the beginning, the structure is apparently more efficient, because the movements are in general smaller. However, although the cap imparts to the *tiburium* a box-like response, the snapshots at longer times make evident the negative effects of the presence of a rigid heavy floor in long-duration earthquakes. Under cyclic loading, the unbalanced thrust from the dome provokes the opening of the drum and the consequent collapse of the surmounting *tiburium*. Not any more supported, the cap falls down on the dome, which catastrophically collapses.

Comparing figure 13*b* with the previous figure 12*b*, one can note again that the $d_{b,z}$ component of displacement for the dot-marked block is almost null, while the $d_{b,x}$ component is much less than in the previous case and follows the oscillations of the ground, because the structure is much

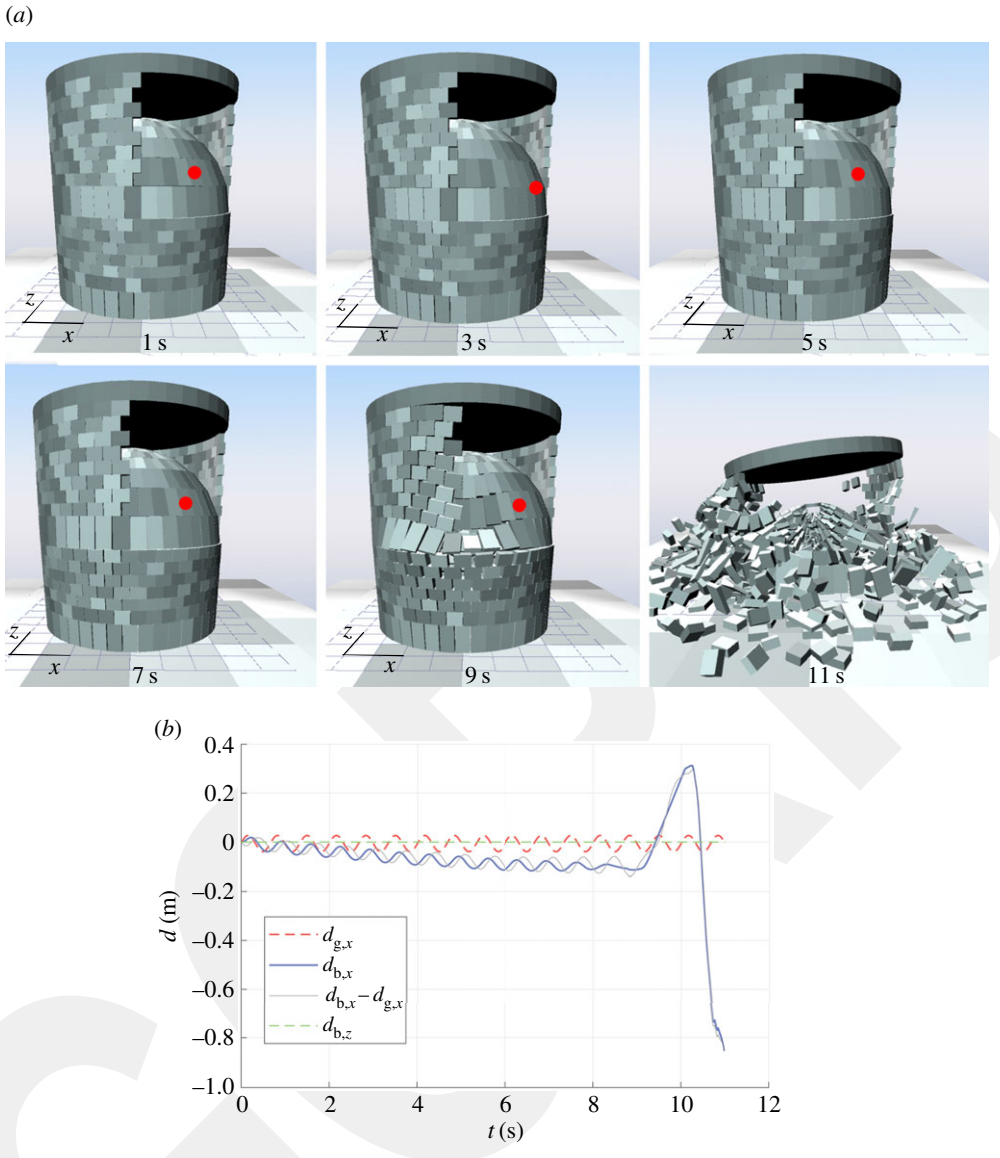

Figure 13. Interlocked dome, drum and *tiburium* closed by a monolithic cap, under *x*-direction oscillatory ground displacement (PGA 0.3 g and $f = 1.5$ Hz). (*a*) Failure steps. (*b*) Comparison of the displacement of the ground ($d_{g,x}$) and of the marked block in *x* ($d_{b,x}$) and *z* ($d_{b,z}$) directions. (Online version in colour.)

stiffer. The displacement sharply increases in the latest stages of the simulation, when the drum and *tiburium* fail and the cap collapses onto the dome.

In further simulations, not recorded here for brevity, the effects of the parameters of the ground motion have been investigated. If the value of the PGA is kept fixed while the amplitude is varied, diminishing the frequencies in general produces a quicker collapse. For example, by changing the frequency from 1.5 to 0.5 Hz, the structure collapses in approximately one-third of the time.

4. Hoop stress and geometric proportions

We address here how the frictional forces interfere with the geometric proportions, both at the local level (the constituent blocks) and at the global level (the shape of the dome).

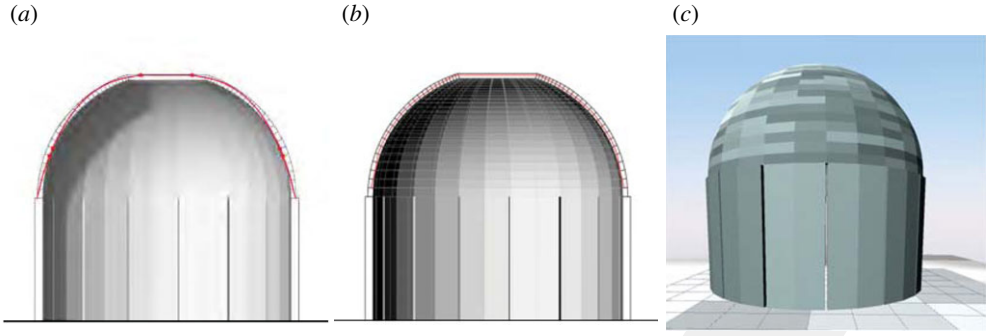

Figure 14. Dome with no *tiburium* made by interlocked flat blocks, supported by a drum with independent slender columns. (*a*) Layout and conventional thrust line. (*b*) Deformation at $t = 1$ s and effective thrust line. (*c*) Deformation at $t = 6$ s. (Online version in colour.)

(a) Widening the blocks: flat tiles

As shown in §3a, the aspect ratio $2h/b$ of the blocks influences the possibility of sustaining hoop stresses through frictional contact. The hemispherical dome of figure 14*a*, for the rest identical to that of figure 5*a*, differs because now the interlocked blocks, with $b = 3$ m and $h = 0.5$ m, have geometric proportions $2h/b = 1/3$. For a friction coefficient $\mu = 0.4$, this respects condition $(3.4)_2$. Superimposed to the section, the same figure also shows the *conventional* thrust line, obtained as if the dome were made by a set of non-interacting lunes, which obviously coincides with that of figure 4*a* and slightly exceeds the profile of the dome. On the other hand, figure 14*b* illustrates the *effective* thrust line at $t = 1$ s, derived from the NSCD simulation as the envelope of the resultants of interface contact forces. Remarkably, this is within the dome profile, and this can only be due to the confining action of the hoop stress from the parallels that produces its centring. Stability is confirmed by the simulation of figure 14*c* that shows the deformation after 6 s.

Some cracks are visible along the meridians and the output of the contact forces confirms that the required hoop stress is only partially equilibrated: a little sliding occurs and the frictional contact reactions cannot exceed the theoretical limit. Further lowering the ratio $2h/b$ could provide a better exploitation of the potentiality of the frictional effects. In any case, this analysis confirms the importance of the correct dimensioning of the bond pattern.

(b) Oval domes

In §3a,b, we have considered spherical domes, illustrating how their horizontal outward thrust, in the occurrence of meridional cracks, can be balanced by the confining action of the drum acting as a chain. As the structure and the weight have cylindrical symmetry, the horizontal outward thrust shares this property, so that the ovalization of the drum is prevented. An oval dome is a dome whose plan has an oval form. In an oval dome, the pie-shaped arches that virtually compose its geometry, when isolated by meridional cracks, have different span-rise ratios, so that their thrusts are different. Therefore, the top of the drum sustaining an oval dome is subjected to non-uniformly distributed horizontal forces.

Figure 15*a* represents the layout of an oval dome obtained by stretching 1.5 times in one horizontal direction the geometry of figure 11, so that its plan[2] is an ellipse, with diameters 14 and 21 m, while height is 7 m for both drum and dome. The interlocked blocks have thickness of 45 cm for the dome ($2h/b = 4$), and 60 cm for both drum and *tiburiua* ($2h/b = 3$). As the slenderness of the blocks forming the dome prevents its full ability to equilibrate tensile hoop stresses, the dome transmits relevant horizontal forces to the top of the drum. In the NSCD simulations, one

[2]These are the basic geometric parameters of the *Sant'Andrea al Quirinale* church in Rome by G. Bernini, even if there the plan is not a perfect ellipse.

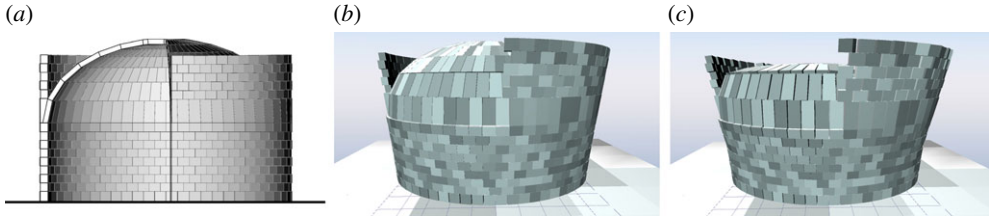

Figure 15. Oval dome made of slender blocks ($h/2b = 4$) and interlocked bond pattern, with 5.8 m high *tiburium*. (*a*) Layout. (*b*) Formation of the mechanics after 1 s. (*c*) Collapse after 2 s. (Online version in colour.)

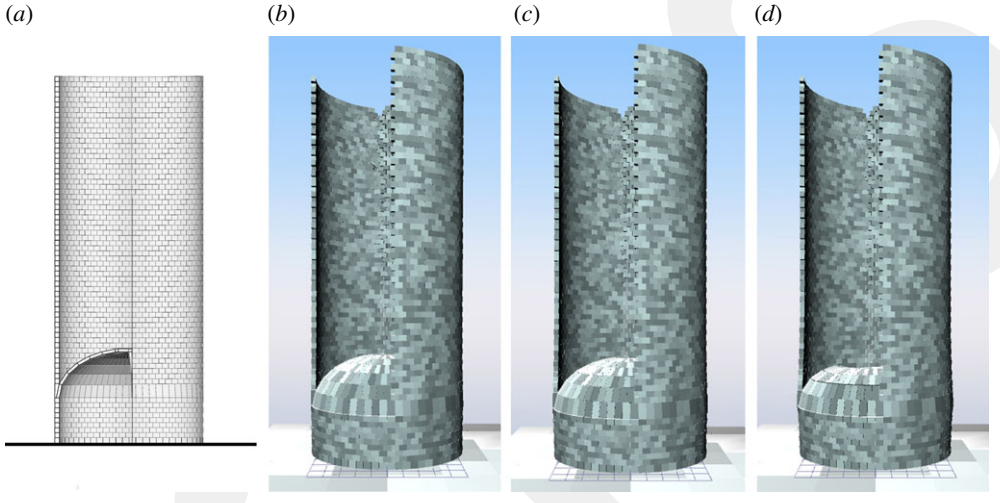

Figure 16. Oval dome with slender blocks ($b/h = 0.5$) and interlocked bond pattern with a 48 m high *tiburium*. (*a*) Layout. Deformation at (*b*) $t = 1$ s, (*c*) $t = 2$ s and (*d*) $t = 16$ s. (Online version in colour.)

notes from figure 15*b* that, just after 1 s from the application of the self-weight, a mechanism starts to form: the oval drum is projected outward by the horizontal forces at those portions where the curvature of its cross section is the lowest (the flattest parts). This is not surprising because the capacity of supporting outward forces in an element with small bending stiffness is proportional to the curvature. Figure 15*c* shows that the dome implodes inwards after 2 s.

A noteworthy improvement can be obtained by increasing the height, and consequently the weight, of the *tiburium*. To illustrate this, figure 16*a* shows the layout of a purely theoretical case, in which the height of the *tiburium* is 48 m. Figure 16*b*,*c* shows again the deformation at $t = 1$ and $t = 2$ s, with some cracks but overall stability. The compression forces transmitted by the *tiburium* on the drum increase not only its effective hoop strength due to frictional contact, but also its resistance to bending actions. As represented in figure 16*d*, it takes about 10 s to reach a collapse mechanism qualitatively similar to that of figure 15*c*, where the drum is pushed outwards at those portions with the lowest curvatures.

The thickness of the dome may also be varied, to produce the desired thrust at the base of the drum. If $a_1 = 10.5$ m and $a_2 = 7$ m are the axes of the ellipse in plan, the curvature in correspondence of the axes is accordingly $\kappa_1 = a_1/a_2^2$ and $\kappa_2 = a_2/a_1^2$. If p_1 and p_2 are the weights *per* unit area of the dome in correspondence of the a_1 and a_2 axes, respectively, one may roughly estimate the thrust *per* unit length here transmitted as $H_1 = p_1 a_1^2/(8f)$ and $H_2 = p_2 a_2^2/(8f)$, with $f = 7$ m being the dome height. By requiring that the horizontal thrust is proportional to the curvature, i.e. $H_1/\kappa_1 = H_2/\kappa_2$, one obtains $p_1/p_2 = a_1/a_2$. Following this, we have diminished

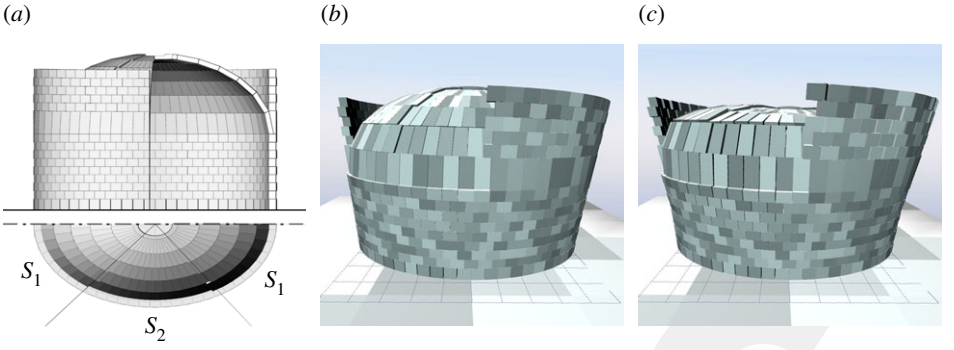

Figure 17. Interlocked oval dome with slender blocks ($2h/b = 4$), with lunes of variable thickness. (*a*) Layout. (*b*) Formation of the mechanism after 1 s. (*c*) Collapse at $t = 2$ s. (Online version in colour.)

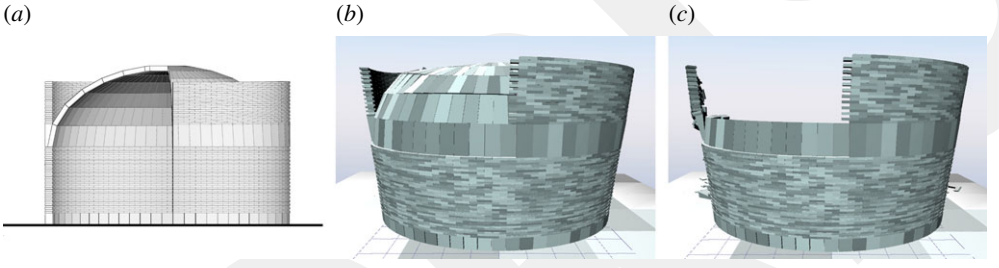

Figure 18. Interlocked oval dome with slender blocks ($2h/b = 4$), drum and *tiburium* with flat blocks ($2h/b = 1/3$) except at the springing. (*a*) Layout. (*b*) Mechanism after 2 s. (*c*) Collapse at $t = 6$ s. (Online version in colour.)

(from 45 to 30 cm) the thickness of the dome in two opposite lunes labelled with S_1 in the plan of figure 17*a*, which are symmetric with respect to the vertical plane containing the minor axis a_2 of the ellipses and form a dihedral angle of approximately 90°. The beginning of the formation of a mechanism after 1 s, as shown in figure 17*b*, is evidenced by localized cracking in the drum. What is remarkable is that a (slightly) better performance is obtained by removing some material. With respect to figure 15*b*, the dome is in fact slightly more stable, but the localized weight reduction is not yet sufficient as figure 17*c* shows the collapse after 2 s. Evidently, it is difficult to achieve a perfect distribution of the thrust forces at the base of the dome, and this is even more complicated by construction tolerances. In any case, the performance could be even better, if the local effect due to the discontinuity of the thickness were eliminated, for example, by smothering the singularity with the introduction of trapezium-shaped blocks.

In order to enhance the effects of frictional forces, one can attempt at enlarging the blocks. In the layout of figures 18*a* and 19*a*, the aspect ratio of the blocks in drum and *tiburium* has been reduced to $2h/b = 1/3$ to satisfy condition $(3.4)_1$. The models are different at the horizontal band in correspondence with the dome springing, which is the same as before in the former layout, subdivided into smaller blocks in the second case. Not much improvement can be achieved, because figures 18*b* and 19*b* prove that after 2 s a collapse mechanism is forming. Both structures collapse after 6 s, as shown in figures 18*c* and 19*c*.

To obtain a stable oval dome, our model predicts that flat blocks should be used for the dome. Figure 20*a* shows blocks with aspect ratio $2h/b = 1/3$, no *tiburium* and a drum formed by independent columns. From figure 20*b*, representing the situation after 1 s, one can observe that meridional cracks start to form in the bond pattern. However, the structure does not collapse, even if the cracks become larger as indicated by figure 20*c*, corresponding to $t = 30$ s.

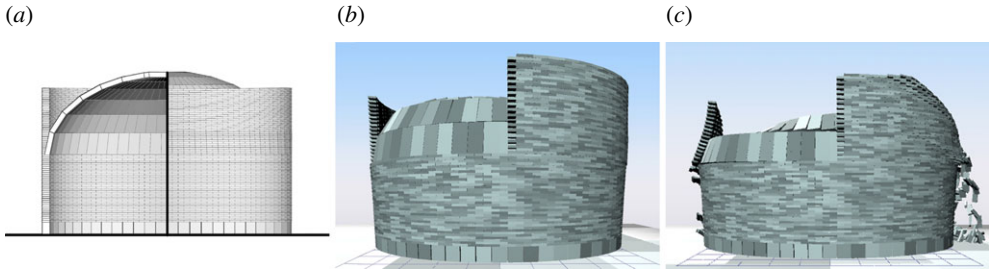

Figure 19. Interlocked oval dome with slender blocks ($2h/b = 4$), drum and *tiburium* with flat blocks ($2h/b = 1/3$) including the springing. (*a*) Layout. (*b*) Mechanism after 2 s. (*c*) Collapse at $t = 6$ s. (Online version in colour.)

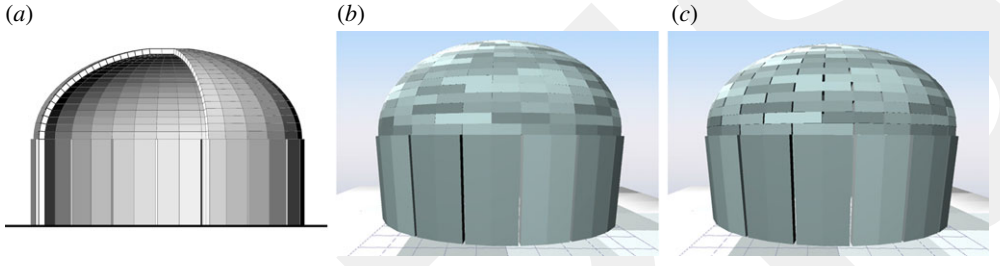

Figure 20. Interlocked oval dome with flat blocks ($2h/b = 1/3$), drum formed by slender columns and no tiburium. (*a*) Layout. (*b*) Deformation after 1 s. (*c*) Cracking but no collapse at $t = 30$ s. (Online version in colour.)

The aforementioned observations are confirmed in the practical example of the elliptical dome of a run-down Orthodox church in Germin (Kayseri, Turkey), represented in figure 21*a*. The internal view from figure 21*b* evidences the sliding of the constituent blocks. The opening of the joints is higher in the lower rings of the dome, where the hoop stress is tensile, and in correspondence of those blocks that are not properly interlocked, i.e. where the end of a block is not above the centre of the block beneath it. Moreover, cracks appear wider at those portions of the drum where the curvature is small.

The dome is a double curvature surface that cannot be deformed when the base is constrained to lay on the horizontal plane represented by the top of the drum. On the other hand, the drum and the *tiburium*, single-curvature (developable) surfaces, can be easily bent by radial forces. Therefore, it is not surprising that in most oval domes of the past, the drum and the *tiburium* are stabilized by strong buttresses to limit their distortion. To investigate this possibility, consider the dome illustrated in the cut-out and the plan of figure 22*a*,*b*, identical to that of figure 19 except for the fact that the less curved portions of the drum are strengthened by six buttresses simply laid on the ground, here modelled as rigid prismatic blocks with the same weight per unit volume of the rest. As results from figure 22*c* showing the deformation after 6 s, the dome is stable because the bulging of the drum, evident in figure 19*c*, is now constrained by the adherent buttresses.

The numerical experiments confirm that the construction of oval domes presents difficulties with respect to domes with cylindrical symmetry, because an oval drum has to resist a distribution of thrusts from the dome that can provoke its bending. The required bending stiffness and strength can be obtained by noteworthy compression, in figure 16, or by adding buttresses as shown in figure 22. In any case, the blocks composing the dome should have a high aspect ratio b/h, to increase their frictional connection. The potential benefit from this interlocking is higher in the dome than in the drum, because the former is a synclastic double curved surface, whereas the latter is a deformable developable surface.

Figure 21. Oval dome of a run-down Orthodox church in Germin (Kayseri, Turkey). (*a*) External and (*b*) internal views. (Online version in colour.)

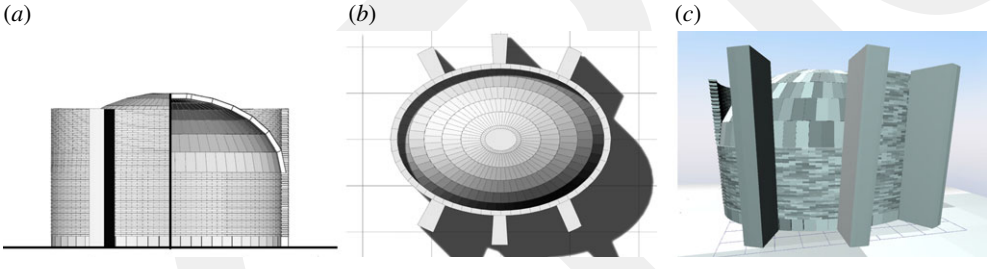

Figure 22. Interlocked oval dome with slender blocks ($2h/b = 4$), drum and *tiburium* with flat blocks ($2h/b = 1/3$) and buttresses. (*a*) Cut-out, (*b*) plan and (*c*) deformation after 6 s. (Online version in colour.)

5. Conclusion

In order to assess the stability of masonry constructions, an NSCD model has been used to discuss the stability of complex assemblies of rigid blocks in frictional contact. The cases considered here are domes, either oval or hemispherical, built on an underlying drum, under static and dynamic loading. We have shown that the stability of these constructions depends on the capacity of the dome and the drum to carry hoop stresses. Unlike the classical approaches, which assume a moderate tensile strength of the bulk material, in our model the resistance to horizontal tensile forces is attributed to the frictional contact between the blocks, which depends on the vertical pressure according to Coulomb's friction law. Because of this, the aspect ratio (height to width) of the constituent blocks plays a crucial role. A *tiburium* built over the drum may further contribute to stabilize the assembly according to two complementary effects: re-centring the line of thrust in the dome and increasing the vertical compression in the drum. This second contribution is important because it can increase the bearing capacity of the drum with respect to hoop stress with the aforementioned frictional mechanism, thus enhancing the stability of the dome. This is particularly effective in the case of oval domes, for which the loss of circular symmetry requires additional stiffness and strength of the drum to equilibrate the uneven thrust forces.

We believe that the present novel approach based on rigid body mechanics and frictional sliding represents a useful complement to the classical no-tensional material modelling. The

capability of investigating the effects of the bond pattern will allow a deeper understanding of the response of complex structures, like for example Brunelleschi's dome in Santa Maria del Fiore, where the role of the herringbone pattern, ingenious from a constructional viewpoint, is still waiting for a reliable structural interpretation. Certainly, the potentiality of the method is yet to be fully explored.

Data accessibility. This work does not have any experimental data.

Authors' contributions. The authors have contributed equally to the preparation of this article.

Competing interests. We have no competing interests.

Funding. V.B. acknowledges the support of Abdullah Gül University, Turkey, under project number FUA-2017-85. G.R.C. acknowledges the support of the Italian Ministry of University under grant MIUR-PRIN voce COAN 5.50.16.01 code 2015JW9NJT and of the Italian Civil Protection Department, Presidency of the Council of Ministers, under project ReLUIS-DPC 2014-2018.

Acknowledgements. The authors are grateful to B. Asiliskender and N. Yoney for their scholarly introduction to interesting historical buildings in Kayseri.

References

1. Kooharian A. 1953 Limit analysis of voussoirs (segmental) and concrete arches. *Proc. American Concrete Institute* **49**, 317.
2. Heyman J. 1995 *The stone skeleton*. Cambridge, UK: Cambridge University Press.
3. O'Dwyer D. 1999 Funicular analysis of masonry vaults. *Comput. Struct.* **73**, 187–197. (doi:10.1016/S0045-7949(98)00279-X)
4. Ochsendorf J. 2002 Collapse of masonry structures. PhD thesis, University of Cambridge, UK.
5. Block P, Lachauer L. 2014 Three-dimensional funicular analysis of masonry vaults. *Mech. Res. Commun.* **56**, 53–60. (doi:10.1016/j.mechrescom.2013.11.010)
6. Akbarzadeh M, Van Mele T, Block P. 2015 On the equilibrium of funicular polyhedral frames and convex polyhedral force diagrams. *CAD Comput. Aided Des.* **63**, 118–128. (doi:10.1016/j.cad.2015.01.006)
7. Marmo F, Rosati L. 2017 Reformulation and extension of the thrust network analysis. *Comput. Struct.* **182**, 104–118. (doi:10.1016/j.compstruc.2016.11.016)
8. Como M. 2013 *Statics of historic masonry constructions*. Berlin, Germany: Springer.
9. Lucchesi M, Padovani C, Pasquinelli G, Zani N. 2008 *Masonry constructions: mechanical models and numerical applications*. Berlin, Germany: Springer Science & Business Media.
10. Gilbert M, Casapulla C, Ahmed H. 2006 Limit analysis of masonry block structures with non-associative frictional joints using linear programming. *Comput. Struct.* **84**, 873–887. (doi:10.1016/j.compstruc.2006.02.005)
11. François M, Royer-Carfagni G. 2005 Structured deformation of damaged continua with cohesive-frictional sliding rough fractures. *Eur. J. Mech., A/Solids* **24**, 644–660. (doi:10.1016/j.euromechsol.2004.12.005)
12. van Zijl G. 2004 Modeling masonry shear-compression: role of dilatancy highlighted. *J. Eng. Mech.* **130**, 1289–1296. (doi:10.1061/(ASCE)0733-9399(2004)130:11(1289))
13. Casapulla C, Portioli F. 2015 Experimental and analytical investigation on the frictional contact behavior of 3D masonry block assemblages. *Constr. Build. Mater.* **78**, 126–143. (doi:10.1016/j.conbuildmat.2014.12.100)
14. Jean M. 1999 The non-smooth contact dynamics method. *Comput. Methods Appl. Mech. Eng.* **177**, 235–257. (doi:10.1016/S0045-7825(98)00383-1)
15. Pang J-S, Stewart D. 2009 Solution dependence on initial conditions in differential variational inequalities. *Math. Program.* **116**, 429–460. (doi:10.1007/s10107-007-0117-5)
16. Pang J-S, Stewart DE. 2008 Differential variational inequalities. *Math. Program.* **113**, 345–424. (doi:10.1007/s10107-006-0052-x)
17. Moreau J-J. 1988 *Unilateral contact and dry friction in finite freedom dynamics*, pp. 1–82. Vienna, Austria: Springer Verlag.
18. Moreau J-J. 1999 Numerical aspects of the sweeping process. *Comput. Methods Appl. Mech. Eng.* **177**, 329–349. (doi:10.1016/S0045-7825(98)00387-9)
19. Acary V, Brogliato B. 2008 *Numerical methods for nonsmooth dynamical systems: Applications in mechanics and electronics*. Lecture Notes in Applied and Computational Mechanics, vol. 35. Berlin, Germany: Springer Verlag.

20. Beatini V, Royer-Carfagni G, Tasora A. 2017 A regularized non-smooth contact dynamics approach for architectural masonry structures. *Comput. Struct.* **187**, 88–100. (doi:10.1016/j.compstruc.2017.02.002)
21. Chetouane B, Dubois F, Vinches M, Bohatier C. 2005 NSCD discrete element method for modelling masonry structures. *Int. J. Numer. Methods Eng.* **64**, 65–94. (doi:10.1002/nme.1358)
22. Rafiee A, Vinches M, Bohatier C. 2008 Application of the NSCD method to analyse the dynamic behaviour of stone arched structures. *Int. J. Solids Struct.* **45**, 6269–6283. (doi:10.1016/j.ijsolstr.2008.07.034)
23. Rafiee A, Vinches M, Bohatier C. 2008 Modelling and analysis of the Nîmes arena and the Arles aqueduct subjected to a seismic loading, using the Non-Smooth Contact Dynamics method. *Eng. Struct.* **30**, 3457–3467. (doi:10.1016/j.engstruct.2008.05.018)
24. Dubois F, Jean M. 2006 *The non-smooth contact dynamic method: recent LMGC90 software developments and application*, pp. 375–378. Berlin, Germany: Springer.
25. Lancioni G, Lenci S, Piattoni Q, Quagliarini E. 2013 Dynamics and failure mechanisms of ancient masonry churches subjected to seismic actions by using the NSCD method: the case of the medieval church of S. Maria in Portuno. *Eng. Struct.* **56**, 1527–1546. (doi:10.1016/j.engstruct.2013.07.027)
26. Lancioni G, Gentilucci D, Quagliarini E, Lenci S. 2016 Seismic vulnerability of ancient stone arches by using a numerical model based on the non-smooth contact dynamics method. *Eng. Struct.* **119**, 110–121. (doi:10.1016/j.engstruct.2016.04.001)
27. Saxcé GD, Feng Z-Q. 1998 The bipotential method: a constructive approach to design the complete contact law with friction and improved numerical algorithms. *Math. Comput. Model.* **28**, 225–245. (doi:10.1016/S0895-7177(98)00119-8)
28. Anitescu M, Tasora A. 2010 An iterative approach for cone complementarity problems for nonsmooth dynamics. *Comput. Optim. Appl.* **47**, 207–235. (doi:10.1007/s10589-008-9223-4)
29. Birgin EG, Martínez JM, Raydan M. 2000 Nonmonotone spectral projected gradient methods on convex sets. *SIAM. J. Optim.* **10**, 1196–1211. (doi:10.1137/S1052623497330963)
30. Heyn T, Anitescu M, Tasora A, Negrut D. 2013 Using krylov subspace and spectral methods for solving complementarity problems in many-body contact dynamics simulation. *Int. J. Numer. Methods Eng.* **95**, 541–561. (doi:10.1002/nme.4513)
31. Coumans E. 2012 Bullet physics web site. http://bulletphysics.org.
32. Gilbert SKEG, Johnson DW. 1988 A fast procedure for computing the distance between complex objects in three-dimensional space. *Robot. Autom.* **4**, 193–203. (doi:10.1109/56.2083)
33. Qu X, Stucker B. 2003 A 3d surface offset method for stl-format models. *Rapid. Prototyp. J.* **9**, 133–141. (doi:10.1108/13552540310477436)
34. Liu C, Zhao Z, Brogliato B. 2008 Frictionless multiple impacts in multibody systems. I. Theoretical framework. *Proc. R. Soc. A: Math. Phys. Eng. Sci.* **464**, 3193–3211. (doi:10.1098/rspa.2008.0078)
35. Tasora A, Anitescu M, Negrini S, Negrut D. 2013 A compliant visco-plastic particle contact model based on differential variational inequalities. *Int. J. Non Linear Mech.* **53**, 2–12. Multibody System Dynamics: A Selective Perspective. (doi:10.1016/j.ijnonlinmec.2013.01.010)
36. Todisco L, Sanitate G. 2016 Static stability of trulli. *Mater. Struct./Mater. et Constructions* **49**, 2893–2905. (doi:10.1617/s11527-015-0693-4)